DOI 10.5162/Ultrasonic2025/A5-a3

Numerical Analysis of Wave Propagation in Partially Saturated Porous Formations for CO_2 Geological Sequestration

Xiumei Zhang[1,2,3], *Yujuan Qi*[1,2,3], *and Lin Liu*[1,2,3]
[1]*State Key Laboratory of Acoustics, Institute of Acoustics, Chinese Academy of Sciences, Beijing 100190, China*
[2]*School of Physics Sciences, University of Chinese Academy of Sciences, Beijing 100049, China*
[3]*Beijing Engineering Research Center of Sea Deep Drilling and Exploration, Institute of Acoustics, Chinese Academy of Sciences, Beijing 100190, China*
zhangxiumei@mail.ioa.ac.cn

Abstract: Understanding elastic wave propagation in unsaturated porous media, critical for geophysical exploration, especially in hydrocarbon reservoirs and CO_2 storage formations, demands accurate numerical frameworks. This study introduces a numerical model based on Lo's three-phase theory to analyze wave dynamics in two-fluid saturated porous media. The governing equations are reformulated into a velocity-stress form and solved using a hybrid algorithm that combines the time-splitting scheme and staggered-grid finite-difference method (FDM), effectively addressing stiffness issues in porous media simulations. Our findings reveal four distinct wave modes: three compressional waves (P1, P2, P3) and one shear wave (S). Notably, slow compressional waves (P2, P3), driven by solid-fluid and fluid-fluid relative motions, show strong dependence on fluid viscosity and frequency. Although these waves are rarely observable at seismic frequencies, their energy distribution and conversion into propagating P1/S waves at interfaces are crucial. Wavefield snapshots demonstrate complex mode conversions among all four waves, reflecting intricate solid-wetting/nonwetting fluid coupling. Key contributions include the algorithm's robustness in simulating multi-wave phenomena, the fluid-phase energy dominance in slow waves, and the complexity of interface-induced mode conversions.

Keywords: numerical simulation, wave propagation, CO_2 geological sequestration, porous media

Introduction

Numerical simulation serves as a vital approach for investigating the acoustic properties of underground reservoirs [1]. Particularly, the staggered-grid finite-difference method (FDM), with high efficiency and low numerical dispersion, has emerged as a primary approach for simulating spatiotemporal characteristics of acoustic wave propagation in complex heterogeneous media.

The porous media framework, considering the solid-fluid coupling effects, provides more accurate representations of acoustic wave propagation in actual geological formations. The efficacy of staggered-grid FDM has been well established through seminal works by Dai et al. [2]. However, significant challenges remain when studying more complex three-phase porous media, such as CO_2 storage reservoirs. Although Lo et al. established a wave theory for unsaturated porous media based on Eulerian formulation [3], which has been successfully applied by other scholars in fluid-containing complex materials and CO_2 geological storage monitoring, numerical simulation research on its acoustic propagation characteristics remains inadequate. Current analyses of spatiotemporal responses in Lo's theory primarily rely on analytical solutions, proving insufficient for practical reservoirs with strong heterogeneity or complex geometries [4]. Therefore, developing a numerical algorithm based on Lo's theory for acoustic responses in porous reservoirs holds substantial theoretical and practical value.

Numerical arithmetic based on Lo's theory

$$\begin{aligned} v_{s(i,j+1/2)}^{x(n+1/2)} &= v_{s(i,j+1/2)}^{x(n-1/2)'} + B_{11} dt D_x \tau_{xx(i,j+1/2)}^{(n)} \\ &\quad + B_{11} dt D_z \tau_{xz(i,j+1/2)}^{(n)} + B_{12} dt D_x \sigma_{1(i,j+1/2)}^{(n)} \\ &\quad + B_{13} dt D_x \sigma_{2(i,j+1/2)}^{(n)}, \\ \tau_{xz(i,j)}^{(n+1)} &= \tau_{xz(i,j)}^{(n)} + \mu dt D_x v_{s(i,j)}^{z(n+1/2)} \\ &\quad + \mu dt D_z v_{s(i,j)}^{x(n+1/2)}, \end{aligned} \tag{1}$$

Based on the previous work of Qi et al., a numerical simulation algorithm for acoustic fields in porous media based on Lo's model was developed using the time-splitting method and the staggered grid finite

DOI 10.5162/Ultrasonic2025/A5-a3

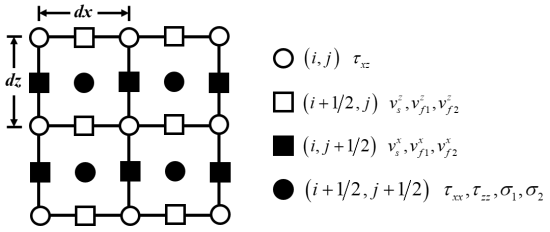

Fig. 1: Spatial distribution of the field variables.

difference method [5][6]. The format of the modified model in two dimensions can be expressed as Eq. (1) and Eq. (2).

$$\begin{aligned}\tau^{(n+1)}_{xx(i+1/2,j+1/2)} &= \tau^{(n)}_{xx(i+1/2,j+1/2)} \\ &+ (a_{11} + 4/3\mu)\, dt D_x v^{x(n+1/2)}_{s(i+1/2,j+1/2)} \\ &+ (a_{11} - 2/3\mu)\, dt D_z v^{z(n+1/2)}_{s(i+1/2,j+1/2)} \\ &+ a_{12} dt \left(D_x v^{x(n+1/2)}_{1(i+1/2,j+1/2)} + D_z v^{z(n+1/2)}_{1(i+1/2,j+1/2)} \right) \\ &+ a_{13} dt \left(D_x v^{x(n+1/2)}_{2(i+1/2,j+1/2)} + D_z v^{z(n+1/2)}_{2(i+1/2,j+1/2)} \right),\end{aligned} \tag{2}$$

where v_g^i indicates the macroscopic average velocity of phase g in i direction; subscript s indicates the phase of solid grain, subscript 1 denotes the phase of nonwetting fluid, and subscript 2 represents the phase of wetting fluid; τ_{ij} indicates the force components of solid grain; σ_i indicates the fluid stress of phase i; a_{ij}, B_{ij} are the coefficients related to Lo's work[3] and Qi's work[6]; dt denotes the time step; Dx and Dz denote the discretized difference operators in the x- and z-directions, respectively. The spatial distribution of the field variables in the staggered-grid finite-difference algorithm is depicted in Fig. 1.

Numerical calculations and analysis

To investigate the spatiotemporal propagation characteristics of waves in unsaturated porous media, the time-splitting staggered-grid finite-difference algorithm is applied to the wave numerical simulation, with the parameters shown in Tab. 1. In the numerical simulation, the model size is 500 m × 500 m, with $dx = dz = 0.2$ m and $dt = 10$ μs. A Ricker wavelet with the dominant frequency of 50 Hz is located at the point (250 m, 250 m), loading on the vertical particle velocity of each phase. Moreover, to mitigate spurious reflections caused by the limited computational domain, the Perfectly Matched Layer (PML) was implemented around the model. Snapshots of the velocity components of the solid grain, the nonwetting and wetting pore fluid at 90 ms are shown in Fig. 2, with a proportional amplitude ratio of each phase. In this case, the influence of fluid viscosity was neglected

Tab. 1: Parameters of unsaturated porous media.

Type	Parameters	Value
Solid grain	grain bulk modulus, K_s (GPa)	40
	frame bulk modulus, K_m (GPa)	7.12
	shear modulus, μ (GPa)	9.986
	grain density, ρ_s (kg/m^3)	2573
	porosity, ϕ	0.135
	permeability, κ (D)	0.706
Nonwetting fluid - CO_2	density, ρ_1 (kg/m^3)	384
	bulk modulus, K_1 (GPa)	0.018
	viscosity, η_1 (mPa · s)	0.028
Wetting fluid - Brine	density, ρ_2 (kg/m^3)	1034
	bulk modulus, K_2 (GPa)	2.65
	viscosity, η_2 (mPa · s)	0.70

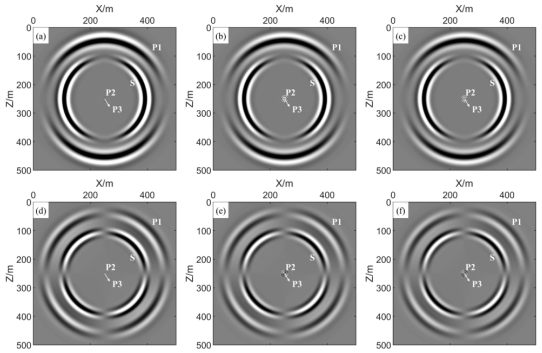

Fig. 2: Snapshots of the vertical particle velocity component of (a) solid grain, (b) nonwetting fluid, and (c) wetting fluid, and the horizontal particle velocity component of (d) solid grain, (e) nonwetting fluid, and (f) wetting fluid at 90 ms.

to magnify the characteristics of the slow compressional waves. It is obviously shown that the P1, S, P2, and P3 waves can be sequentially observed from outer to inner regions. Especially, the energy of the P3 wave is concentrated near the source, due to its slow velocity. Additionally, the phase contrast reveals that the P2 wave is generated by the relative motion between the solid grain and pore fluids, while the P3 wave is generated due to the relative motion between the nonwetting fluid and wetting fluid. The P2 and P3 waves concentrate their energy in the phase of pore fluids.

To clarify the conversion process of acoustic waves at the interface, a two-layer unsaturated porous media model is constructed, and the model parameters are shown in Tab. 2. To ensure that the results are

DOI 10.5162/Ultrasonic2025/A5-a3

Tab. 2: Parameters for modeling two-layer, three-phase porous media

Type	Parameters	Upper layer	Lower layer
Solid grain	grain bulk modulus, K_s (GPa)	40	40
	frame bulk modulus, K_m (GPa)	1.37	9.50
	shear modulus, μ (GPa)	0.82	6.20
	grain density, ρ_s (kg/m^3)	2600	2800
	porosity, ϕ	0.36	0.2
	permeability, κ (D)	1.6	8
Non-wetting fluid	density, ρ_1 (kg/m^3)	498	860
	bulk modulus, K_1 (GPa)	0.025	1.3
	viscosity, η_1 (mPa · s)	0.035	300
	Saturation, S_1 (%)	80	50
Wetting fluid	density, ρ_2 (kg/m^3)	1036	1036
	bulk modulus, K_2 (GPa)	2.64	2.64
	viscosity, η_2 (mPa · s)	0.77	0.77
	Saturation, S_2 (%)	20	50

accurate with the boundary conditions of layered interfaces, the parameters at the interfaces are effectively averaged[7].

In the numerical simulations, a P-wave source with a dominant frequency of 30 kHz is applied at (0.4 m, 0.3 m) to excite the vertical particle velocity in each phase. Fig. 3 displays snapshots of the vertical particle velocity across different phases, clearly showing direct P1 and P2 waves, along with various converted waves, including reflected waves and transmitted waves. The comparison between solid and fluid wavefields reveals that converted slow waves exhibit stronger signatures in the fluid phase, demonstrating significant phase-dependent energy conversion at the interface. Notably, the P3 wave remains localized near both the source and interface due to its slow propagation velocity. Furthermore, when the slow compressional wave crosses the interface, it converts into fast compressional and shear waves that continue to propagate normally, highlighting the complex wave conversion processes occurring in the unsaturated porous media.

Vertical Seismic Profiling (VSP) is a seismic monitoring technique, provides higher resolution and finer details of the subsurface structure due to the receivers being located inside the well. Therefore, the time-lapse VSP surveys are modeled. The classical block model saturated with brine is established with Tab. 3. Layers A and C represent formations with poor porosity and permeability, and layer B represents the target

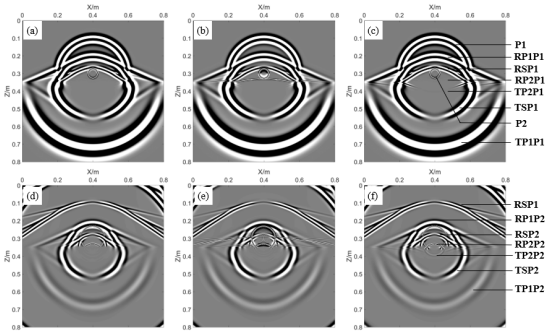

Fig. 3: Snapshots of the vertical particle velocity component of (a, d) solid grain, (b, e) nonwetting fluid, and (c, e) wetting fluid at 0.2 ms and 0.5 ms, respectively.

Tab. 3: Parameters of the solid grain of a horizontally laminated formation.

Layer Number	A	B	C
grain bulk modulus, K_s (GPa)	40.33	40	40
frame bulk modulus, K_m (GPa)	12.6	7.12	23.9
shear modulus, μ (GPa)	12.3	9.986	16
grain density, ρ_s (kg/m^3)	2704	2226	2670
porosity, ϕ	0.019	0.135	0.016
permeability, κ (D)	0.1472	0.7063	0.0001

reservoir for CO_2 injection.

In numerical simulations, a single P-wave source is used, with receivers located at depths 100 m - 1260 m, spaced 4 m apart. Fig. 4 shows the corresponding seismograms as the injected S_{CO2} is 0.4. Both the upgoing and the downgoing wavefields are observed. The intersection point of wave conversion matches the positions of the layer interfaces, which can be used for stratigraphic calibration.

The waveforms from depths of 700 m and 1000 m are subject to decimation for detailed analysis. Fig. 5 shows the comparison under different injected S_{CO2}. The variation of CO_2 can be observed by time-lapse arrival times of the reflected and transmitted waves, particularly the compressional waves. In this scenario, the difference between injected S_{CO2} is 0% and 5% is minimal. At this time, CO_2 is mainly dissolved into the brine, resulting in lower free S_{CO2}. Additionally, the acoustic response becomes more pronounced while free S_{CO2} increases, particularly showing the decrease in compressional velocity and the delay of travel time. As expected, the acoustic methods can effectively

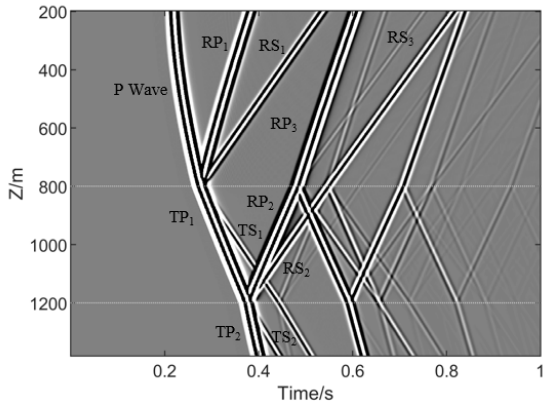

Fig. 4: Corresponding seismograms with $S_{CO2} = 0.4$ in layer B

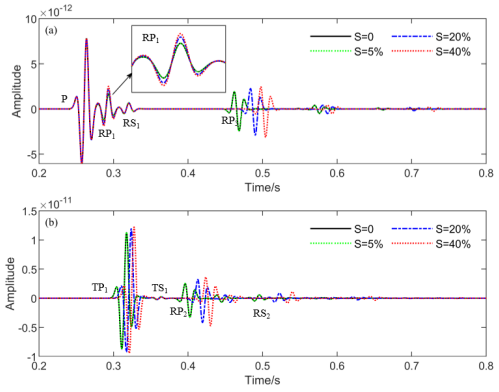

Fig. 5: Received waveforms for different injected S_{CO2} in layer B: (a) Z = 700 m; (b) Z = 1000 m.

detect the migration of free-phase CO_2. However, the process of dissolution seems impossible to detect.

Conclusion

In this paper, we analyze the wave propagation characteristics in porous media saturated with CO_2 and brine. Using the time-splitting staggered-grid finite-difference algorithm, we efficiently obtained the wavefield snapshot and waveforms in unsaturated porous media. The energy distribution and generation mechanism of various types of waves in unsaturated porous media, as well as the acoustic wave mode conversion at the interface, have been systematically analyzed. Synthesizing the study, we undertake a comparative exploration of VSP responses within saline aquifers, while considering variations in CO_2 saturation.

The proposed numerical algorithm allows us to effectively illustrate the transmission process of four waves in unsaturated porous media. At seismic frequencies, only P1 and S waves are considered propagating waves, while P2 and P3 waves are identified as diffusion waves influenced by the viscous coefficient. The propagation behavior and energy distribution at the interface vary significantly across different components, highlighting the strong coupling between the solid grain, wetting fluid, and non-wetting fluid. This coupling must be considered when assessing wave attenuation. Moreover, a series of waveforms for VSP monitoring has been modeled to account for both CO_2 saturation and dynamic fluid effects. The results indicate that an increase in free S_{CO2} corresponds to a time delay in arrivals.

References

[1] J. M. Carcione, C. Morency, and J. E. Santos. "Computational poroelasticity—A review". In: *Geophysics* 75.5 (2010), 75A229–75A243. DOI: 10.1190/1.3474602.

[2] N. Dai, A. Vafidis, and E. Kanasewich. "Wave propagation in heterogeneous, porous media: A velocity-stress, finite-difference method". In: *Geophysics* 60.2 (1995), pp. 327–340. DOI: 10.1190/1.1443769.

[3] W. C. Lo, C. L. Yeh, and J. W. Lee. "Effect of viscous cross coupling between two immiscible fluids on elastic wave propagation and attenuation in unsaturated porous media". In: *Advances in water resources* 83 (2015), pp. 207–222. DOI: 10.1016/j.advwatres.2015.06.002.

[4] Y. Zhang and P. Ping. "Nonmonotonic traveling waves in an unsaturated medium induced by a solid force and fluid mass sources". In: *Advances in Water Resources* 142 (2020), p. 103633. DOI: 10.1016/j.advwatres.2020.103633.

[5] J. M. Carcione and G. Quiroga-Goode. "Some aspects of the physics and numerical modeling of Biot compressional waves". In: *Journal of Computational Acoustics* 3.04 (1995), pp. 261–280. DOI: 10.1142/S0218396X95000136.

[6] Y. Qi, X. Zhang, and L. Liu. "The elastic wave propagation in Lo's three-phase porous media theory-based time-splitting staggered-grid finite-difference method". In: *Journal of Geophysics and Engineering* 22.2 (2025), pp. 399–416. DOI: 10.1093/jge/gxaf012.

[7] W. Guan and H. Hu. "The parameter averaging technique in finite-difference modeling of elastic waves in combined structures with solid, fluid and porous subregions". In: *Communications in Computational Physics* 10.3 (2011), pp. 695–715. DOI: 10.4208/cicp.020810.161210a.